4

Results and Discussion

4.1 Selection of medicinal plant and isolation of essential oil

The traditional medicinal plant, *Kaempferia galanga L.* also known as aromatic ginger was selected for the present study based on its extensive use in the folk medicine culture of Meghalaya. The essential oil was isolated from the rhizome part of the aromatic ginger plant *Kaempferia galanga* L. by using Soxhlet apparatus. The extraction was carried out using hexane as a solvent. Once the Soxhlet extraction process was over, the extracted yield was concentrated using a rotary vacuum evaporator. The concentrated extract was further allowed to dry until no further evaporation was observed. The final extract contained only the essential oil without any solvent. The final yield of the essential oil obtained after extraction was found to be 7.56% (Fig. 4.1)
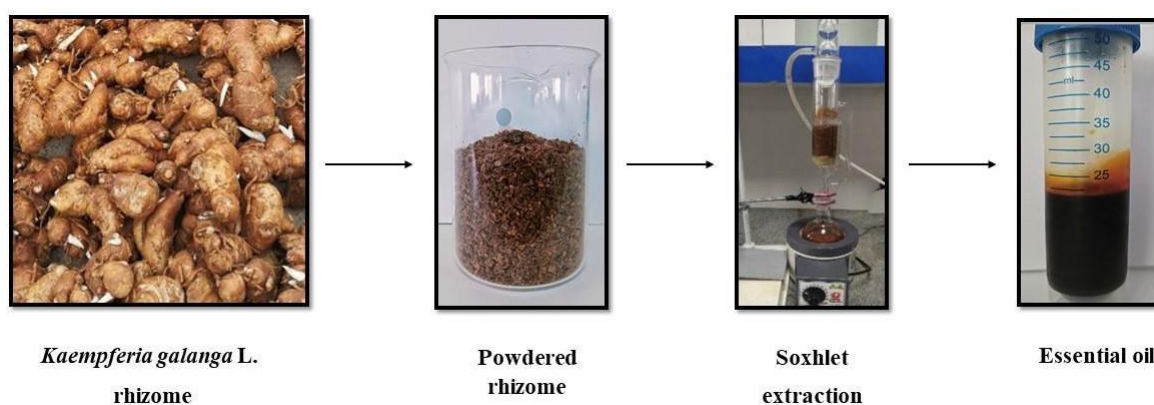

Kaempferia galanga L.   Powdered   Soxhlet   Essential oil
rhizome   rhizome   extraction

Fig. 4.1 Isolation of *Kaempferia galanga* L. essential oil using Soxhlet apparatus

4.2 Characterization of essential oil

The essential oil obtained was further characterized using GC-MS to identify the contents of the essential oil. This led to the identification of eleven major compounds: linalool, cis-Verbenol, citral, γ-Elemene, γ-Muurolene, germacrene D, β-Humulene,

caryophyllene, isocaryophyllene, aromandendrene and alloaromadendrene oxide. The compounds from the gas chromatogram identified from NIST library with respective MS peaks are shown in Fig. 4.2 and tabulated in Table 4.1. The main constituents detected were γ-Muurolene and germacrene D (11.04%) and Citral (1.81%). All the identified compounds belonged to various chemical groups and most of them are known to possess significant biological and pharmacological activities [245]. Other workers revealed the presence of various compounds such as linoleoyl chloride, caryophyllene oxide, cubenol, caryophyllene etc., from Bangladesh [246]. It was reported the presence of borneol, 2-propenoic acid, murolene, caryophyllene oxide and ethyl p-methoxycinnamate from the essential oil of the leaves of the *K. galanga* plant obtained from Odisha, India. Different studies reveal variations in *K. galanga* essential oil's chemical composition due to environmental factors, sampling time, plant genetics, vegetative phases, and extraction methods [247]. MS eluted peaks of different retention time has been attached in the appendices.
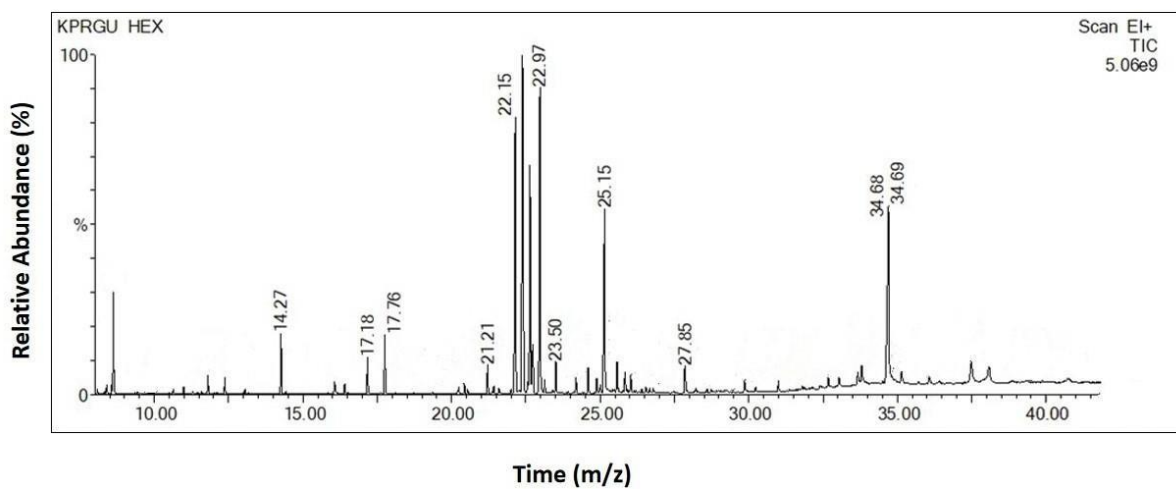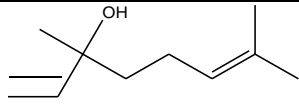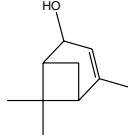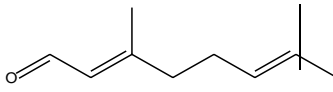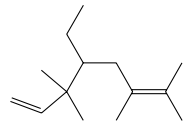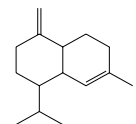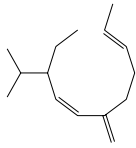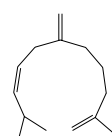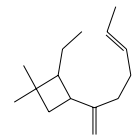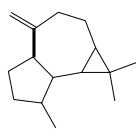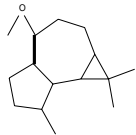

Fig. 4.2 Total Ion Chromatogram (TIC) of the *Kaempferia galanga* L. essential oil obtained after GC-MS analysis

Table 4.1 GC-MS characterized compounds of *Kaempferia galanga* L. essential oil

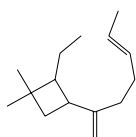| Sl. No	Retention time	M.W	Abundance %	Relative Abundance %	Compound name	Structure
1	14.27	154	11.04	1.75	Linalool ($C_{10}H_{18}O$)	
2	17.18	152.23	6.81	1.08	cis-Verbenol ($C_{10}H_{16}O$)	
3	17.76	152	11.41	1.81	Citral ($C_{10}H_{16}O$)	
4	21.21	204	5.85	0.93	γ-Elemene ($C_{15}H_{24}O$)	
5	22.97	204	69.70	11.04	γ-Murolene ($C_{15}H_{24}O$)	
6	22.97	204.35	69.70	11.04	Germacrene D ($C_{15}H_{24}O$)	
7	23.50	204.35	5.92	0.94	β-Humulene ($C_{15}H_{24}O$)	
8	23.50	204.35	5.92	0.94	Caryophyllene ($C_{15}H_{24}O$)	
9	23.50	204.35	5.92	0.94	Isocaryophyllene ($C_{15}H_{24}O$)	
10	23.50	204.35	5.92	0.94	Aromandendrene ($C_{15}H_{24}O$)	
11	27.85	220.35	8.16	1.29	Alloaromadendrene Oxide ($C_{15}H_{24}O$)	

4.3 Phytochemical evaluation of the essential oil

The phenol and flavonoid content of the essential oil obtained from the plant was found to be 1.38±0.01 and 0.75±0.01 µg/ml GAE and QE per 1mg of fresh weight respectively as tabulated in Table 4.2. Quantitative determination of *Kaempferia galanga* L. rhizomes contained considerable amount of phenolic and flavonoid content thereby making the plant useful for the formulation of the different drug formulations for human uses for treating various diseases [248]. *K. galanga* L. can scavenge reactive oxygen intermediates without oxidative reactions, revealing it as a rich source of phenolics, flavonoids, and natural antioxidants. The phenolic content of the plant may be influenced by factors like extraction method and phenological stage. The flavonoid content is influenced by the location of the sample and dominant climatic and environmental factors [249].

Table 4.2 Phytochemical analysis of *Kaempferia galanga* L. essential oil

Total Phenolic µg/ml GAE per 1mg of fresh weight	Total Flavonoid µg/ml QE per 1mg of fresh weight
1.38±0.01	0.75±0.01

*mg.GAE/g.DW: (mg of gallic acid equivalent per g dry weight).

*mg.QE/g.DW: (mg of quercetin equivalent per g dry weight).

4.4 Antioxidant activity (*In- vitro* radical scavenging assay)

The antioxidant potential of the *K. galanga* L. essential oil, as evaluated from the 2,2-diphenyl-1- picrylhydrazyl (DPPH) assay scavenging, 2,29-azinobis-(3-ethylbenzothiazoline-6-sulfonic acid) (ABTS$^{.+}$) and Phosphomolybdenum assays, revealed promising antioxidant properties (Tables 4.3 and 4.4). From the data, it has been observed that with the increased concentrations of oil, antioxidative activity of scavenging the free radicals increased (Fig. 4.3 and 4.4). Lower IC_{50} value reflects higher radical scavenging activity. *Kaempferia galanga* L. E.O. was capable of scavenging ABTS$^{.+}$ and DPPH in a concentration dependent manner, having IC_{50} value of 38.75 and 36.47 µg/ml. The p-value was found to be 0.0019 and 0.00009 respectively, depicting the results are highly significant. TAC results reveal the

antioxidant activity of essential oil at 46.16 µg/ml concentration. Antioxidant activity prevents the formation of initiator radicals and helps in termination of in chain propagation, or indirectly enhances enzyme activities to remove reactive species or induces their expression. The antioxidant activity of essential oils is typically a result of the synergistic effect of their various constituents. The study found that essential oil obtained from *Kaempferia galanga* L. has effectively inhibited the DPPH and ABTS$^{\cdot+}$ radical, demonstrating better IC$_{50}$ values, thus they can be considered as potential antioxidant compounds.

In the present study, the essential oil was found to contain high levels of phenolic content, which may contribute to the antioxidant properties. Phenolic compounds are considered as antioxidants due to their high reactivity towards peroxyl radicals and suggests their potential use as natural antioxidant sources, as reactive oxygen species can damage nucleic acids, proteins, and lipids [250].

Table 4.3 Free radical scavenging activity of *Kaempferia galanga* L. essential oil by DPPH assay depicting the half minimal inhibitory concentration.

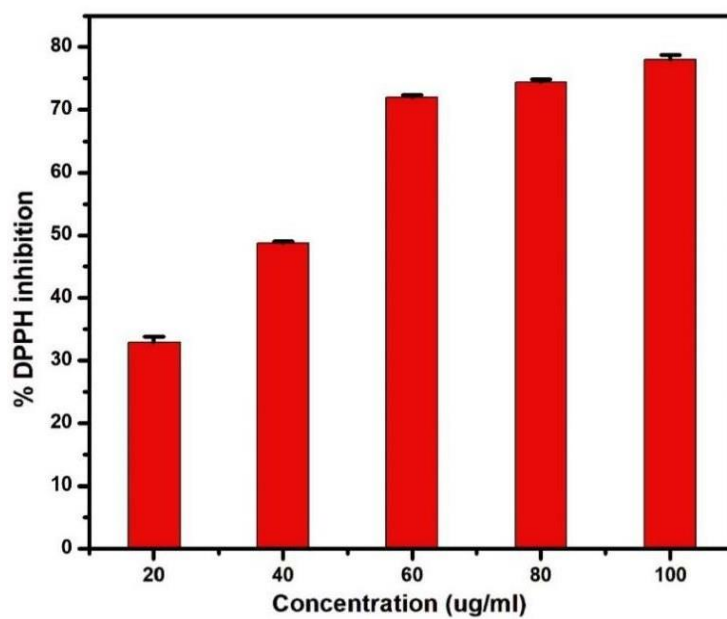| Concentration (µg/ml)	% Free radical Scavenging Activity	IC$_{50}$
20	32.92±0.84	
40	52.38±0.29	
60	71.95±0.36	38.57
80	74.39±0.41	
100	78.04±0.7	

Fig. 4.3 Free radical scavenging activity of the essential oil of *Kaempferia galanga* L. by DPPH assay

Table 4.4 Free radical scavenging activity of *Kaempferia galanga* L. essential oil by ABTS$^{\cdot+}$ depicting the half minimal inhibitory concentration.

Concentration (µg/ml)	% Free radical Scavenging Activity	IC$_{50}$
25	43.43±0.7	
50	58.16±0.4	
75	65.25±0.7	36.47
100	78.12±0.86	
125	85.77±0.6	
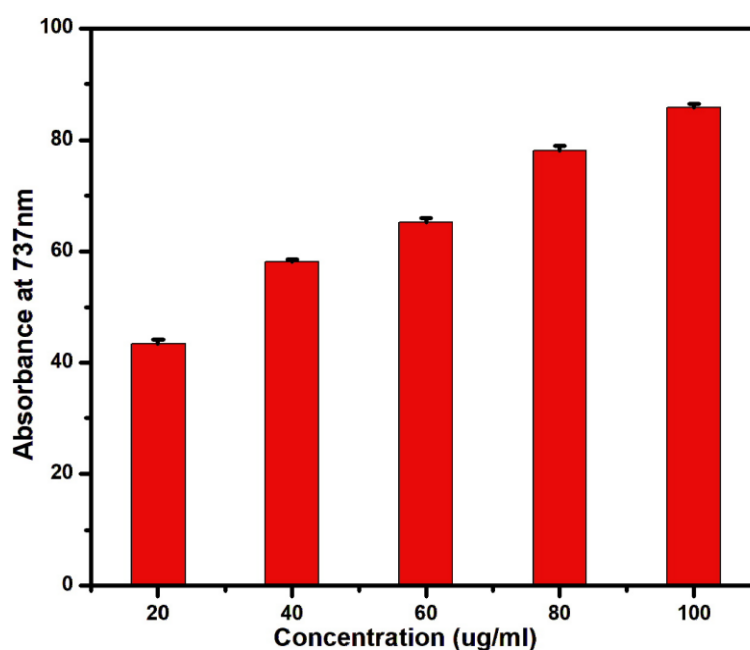
Fig. 4.4 Free radical scavenging activity of the essential oil of *Kaempferia galanga* L. by ABTS$^{\cdot+}$ assay

4.5 Cytotoxicity analysis of essential oil

The *in vitro* haemolytic activity was carried out to determine the cytotoxicity of *Kaempferia galanga* L. essential oil using red blood cells. It has been observed that at concentrations of 0.02, 0.04, 0.06, 0.08 and 0.1 mg/mL respectively, the percentage of haemolysis ranged from 3.21 to 4.18% (Table 4.5 and Fig. 4.5). The p-value was found

to be 0.0001 depicting the results are highly significant. The haemolysis study demonstrates the potential damage to erythrocyte membranes, which release haemoglobin during lysis [251].

It is reported that haemolysis values up to 10% is considered non-toxic to erythrocyte membrane, 10 to 49% slightly toxic, 50 to 89% toxic, and 90 to 100% as highly toxic [252]. The ointment formulated was primarily used for topical application for wound healing, but it's crucial to understand its potential for substance penetration into tissues and toxic effects. In the present study, the toxicity of the essential oil on human erythrocytes was carried out to investigate if the oil may alter the fluidity of cell membranes and thus allow other substances to enter the cells. However, depending upon the concentration and interactions with membrane receptors, it was found that the essential oil did not cause any cell damage and thus found to be non-toxic to erythrocyte [253-255].

Table 4.5 Haemolytic activity of *Kaempferia galanga* L. essential oil

Concentration (mg/ml)	Haemolysis (%)
0.02	3.21±0.62
0.04	3.42±0.63
0.06	3.87±0.56
0.08	4.08±0.41
0.1	4.18±0.35
PBS	0.01±0.86
Triton X-100	100±0.63

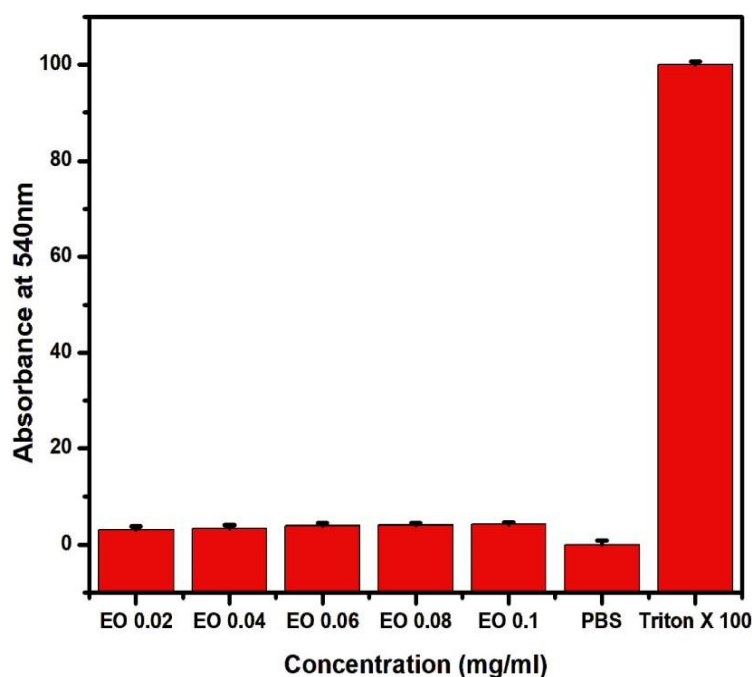**Fig. 4.5** Haemolytic activity of *Kaempferia galanga* L. essential oil

4.6 Antimicrobial screening

4.6.1 Well diffusion assay and Minimum Inhibitory Concentration

The essential oil of *K. galanga* L. exhibited a clear zone of inhibition against *S. aureus* with an inhibition zone of 27±0.21mm as against 37±1.15 demonstrated by the positive control chloramphenicol (Table 4.6 and Fig. 4.6) while the MIC tests revealed

inhibition of the bacterial growth at 2.5 µg/ml for *S. aureus* (Table 4.6 and Fig. 4.7). This suggests that, the oil diffused into and damaged the cell membrane structures for the gram-positive bacteria thereby lowering its activity [256]. The study reveals that *S. aureus,* a gram-positive bacterium is sensitive to the essential oil [257, 258].

The study on EOs' antibacterial mechanism reveals that they directly act on cell membranes, destroying structure and increasing permeability, leading to bacterial cell death. Additionally, EOs may interact with lipophilic membrane and isolated mitochondria, disrupting their integrity and function. Thus, EOs may have multiple ways to affect microbial cells [259,260].

Membrane potential (MP) is a crucial factor in bacterial metabolism, and its decrease can be caused by structural damage to the cell membrane. Addition of EO indicates cell membrane depolarization, leading to decreased metabolic viability and bacterial death [261,262]. Proteins are essential biological macromolecules found in bacterial cell membranes and cytoplasm. The hydrophobicity of EOs interferes with the synthesis of bacterial lipid membranes, causing increased permeability and protein leakage and this is related to phenolic compounds in EOs. EO treatment causes protein leakage in bacterial cells by destroying the membrane, reducing protein content, and interfering with protein synthesis. This reduces protein expression, exerting its antibacterial activity [263,264].

Studies have revealed that essential oils (EOs) can alter the integrity of cell membranes, leading to the loss of vital intracellular contents like proteins, reducing sugars, ATP, and DNA. They also inhibit energy generation and enzymes, causing cell destruction and electrolyte leakage. The antimicrobial activity of EOs is attributed to a cascade of reactions involving the entire bacterial cell [265-267].

Table 4.6 Antimicrobial screening of *Kaempferia galanga* L. essential oil against *S. aureus*

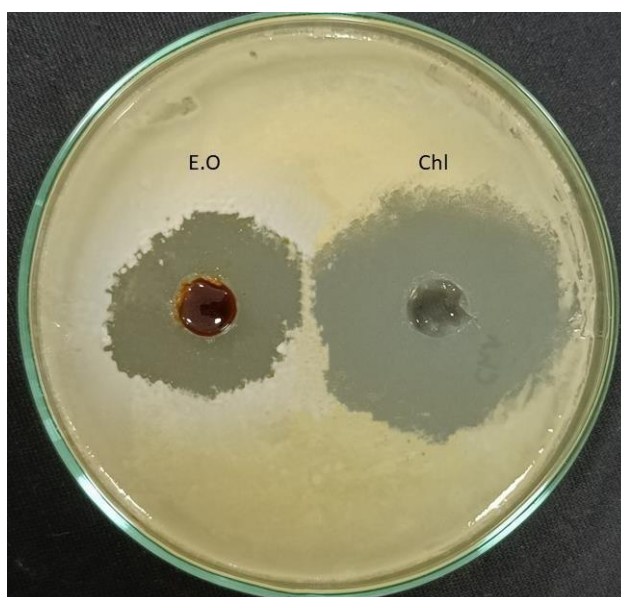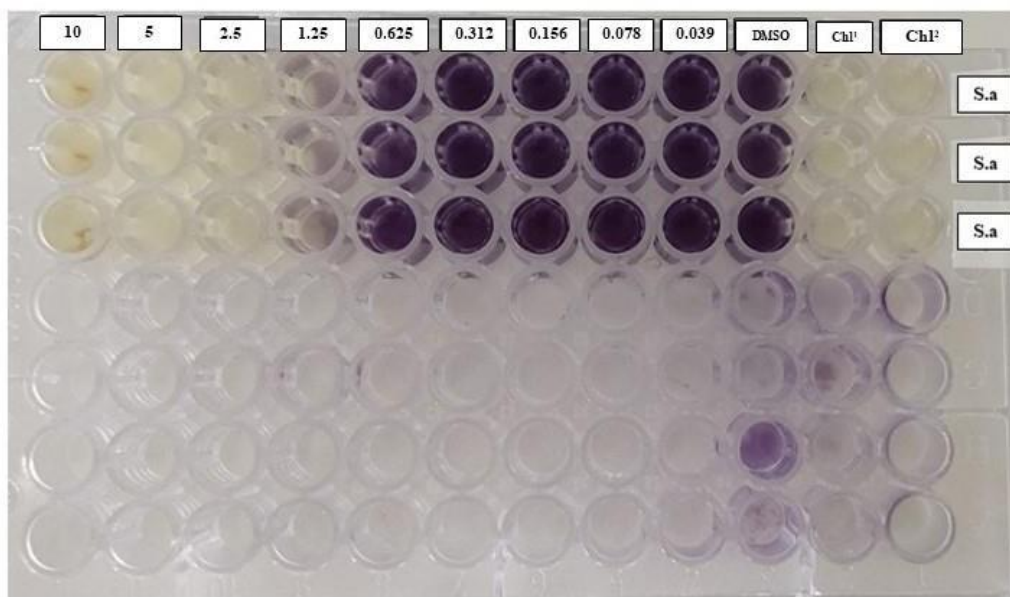| Microbial Strain	Agar Well Diffusion (mm)		Minimum Inhibitory Concentration (µg/ml)
	Essential oil (mg/ml)	Chloramphenicol (mg/ml)	
Staphylococcus aureus	27±0.5	37±1.15	2.5 ±0.01

Fig. 4.6 Agar well diffusion assay of essential oil against *Staphylococcus aureus*

*Chl¹= Chloarmphenicol (125μg/ml), Chl²= Chloarmphenicol (250μg/ml), DMSO= Dimethyl sulphoxide, S.a= *Staphylococcus aureus*

- Concentration is expressed as μg/ml

Fig. 4.7 MIC activity of essential oil against *Staphylococcus aureus*

4.6.2 Antibiofilm inhibition

The essential oil inhibited biofilm formation at a rate of 42-50% at different concentration ranges of 0.25mg/ml to 1 mg/ml (Table 4.7 and Fig. 4.8). The p-value was found to be 0.0001 depicting the results are highly significant. The oil could have interacted with bacterial surface proteins, compromising the initial connection phase and interfering with quorum sensing systems. The success of inhibiting cellular link can be attributed to the favourable environment for bacterial fixation during the initial stage of biofilm formation with surface conditioning. Therefore, the anti-biofilmproperties of the essential oil reflect its antimicrobial activities which thereby supportsthe use of essential oil in various traditional treatment regimens [268-270].

Table 4.7 Antibiofilm activity of *Kaempferia galanga* L. against *S. aureus*

Concentration (mg/ml)	% Biofilm Inhibition
0.25	42.77±1.06
0.50	44.54±0.77
0.75	46.90±0.88
1	50.44±1.01
G1	61.65±1.23
M1	0.08±0.95
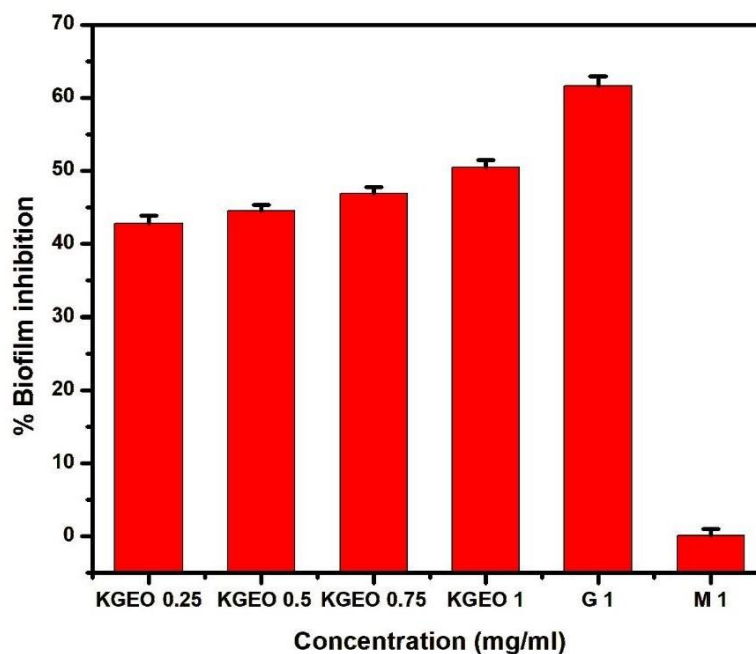
Fig. 4.8 Biofilm inhibition of essential oil against *Staphylococcus aureus*

4.7 In-silico investigations of bioactive compounds

4.7.1 Absorption, Distribution, Metabolism, Excretion, and Toxicity (ADMET) analysis

The drug properties of the compounds were screened according to Lipinski's rule of five and ADMET properties for the drug likeliness. The compounds that acquired the Lipinski rule of five *viz.*, Lipinski molecular weight (MW) ≤ 500, octanol/water partition coefficient (A log P) ≤ 5, number of hydrogen bond donors (HBDs) ≤ 5, number of hydrogen bond acceptors (HBAs) ≤ 10.6, and, molar refractivity should be

between 40-130, were linalool, cis-verbenol, citral, γ-elemene, germacrene D, β-humulene, caryophyllene, isocaryophyllene, aromandendrene and alloaromadendrene oxide. The Lipinski satisfied compounds, were then screened for their ADMET properties depicted in Table 4.8. The ADMET analysis of the compounds indicated were found to have better water solubility while they demonstrated varied results in terms of distribution through blood brain barrier. The compounds were found to have total clearance from the system and were non-hepatotoxic. As such the study reveals that the bioactive compounds present in *K. galanga* L. have drug properties without any disturbance in the normal habitat of human internal conditions which was confirmed by the Lipinski rule of five and ADMET properties [271].

Table 4.8 ADMET properties of the compounds isolated from *Kaempferia galanga* L. essential oil

Compound ID	Alloaromadendrene oxide (1)	Aromendendrene	Isocaryophyllene	Caryophyllene	β-Humulene	Germacrene-D	γ-Murrolene	γ-Elemene	Citral	cis-Verbenol	Linalool	
Caco2 permeability (log Papp in 10^{-6} cm/s)	1.491	1.395	1.423	1.423	1.421	1.436	1.427	1.405	1.504	1.476	1.493	Absorption
Intestinal absorption (human)(% Absorbed)	95.801	95.302	94.845	94.825	94.682	95.59	96.475	93.381	95.317	94.833	93.163	
P-glycoprotein substrate	N	N	N	N	Y	N	N	N	N	N	N	
P-glycoprotein I inhibitor	N	N	N	N	N	N	N	N	N	N	N	
P-glycoprotein II inhibitor	N	N	N	N	N	N	N	N	N	N	N	
CNS permeability (log PS)	-2.114	-1.769	-2.172	-2.172	-2.555	-2.138	-1.631	-1.641	-1.986	-2.468	-2.339	Distribution
CYP2D6 substrate	N	N	N	N	N	N	N	N	N	N	N	
CYP3A4 substrate	Y	Y	N	N	N	N	N	Y	N	N	N	
CYP1A2 inhibitor	N	N	N	N	N	N	N	N	N	N	N	
CYP2C19 inhibitor	N	N	N	N	N	N	N	N	N	N	N	Metabolism
CYP2C9 inhibitor	N	N	N	N	N	N	N	N	N	N	N	
CYP2D6 inhibitor	N	N	N	N	N	N	N	N	N	N	N	
CYP3A4 inhibitor	N	N	N	N	N	N	N	N	N	N	N	
Renal OCT2 substrate	N	N	N	N	N	N	N	N	N	N	N	Excretion
AMES toxicity	N	N	N	N	N	N	N	N	N	Y	N	
hERG I inhibitor	N	N	N	N	N	N	N	N	N	N	N	
hERG II inhibitor	N	N	N	N	N	N	N	N	N	N	N	Toxicity
Oral Rat Acute Toxicity (LD50) (mol/kg)	1.537	1.526	1.617	1.617	1.766	1.634	1.54	1.514	1.815	1.769	1.704	

4.7.2 Molecular docking assay

The *in silico* docking study was conducted to understand the mechanism as to how the bioactive compounds isolated from the essential oil caused inhibition of biofilmforming proteins in *Staphylococcus aureus*.

From the molecular docking analysis, it was observed that the compound γ-elemene showed the best binding affinity with CrtM with binding energy −8.1 kcal/mol whereas caryophyllene and its derivative isocaryophyllene showed the best binding with SarA with binding energy −6.1 kcal/mol. The best binding analysis were represented by the lower binding energy. The detailed docking results of each compound against both the target proteins are shown in the Table 4.9. Since isocaryophyllene is the derivative of caryophyllene, we used caryophyllene only for MD simulation. The two-dimensional (2-D) structure of protein-ligand interactions of γ-elemene with CrtM and caryophyllene with SarA are depicted in the Fig. 4.9. The molecular docking studies predicted the ability of γ-Elemene and caryophyllene to interact better amongst the rest of the compounds against CrtM and SarA target protein. γ-Elemene, formed non-covalent interactions with CrtM at the amino acid residues Phe 26, Val 137, Leu 164, Ala 134, and Phe 22. Similarly, caryophyllene formed non-covalent interactions with SarA at the amino acid residue Ile 132 as shown in Fig. 4.9. These results imply that the binding of γ-Elemene and caryophyllene to the active sites of target proteins involved in staphyloxanthin biosynthesis and virulence factor resulting in adhesion and tissue spread respectively, could be a possible mechanism responsible for the biofilm inhibition in *Staphylococcus aureus*. The best binding complexes of both the cases were subjected to MD simulation analysis.

Table 4.9 Binding affinity of the characterized compounds of *Kaempferia galanga* L. with CrtM (PDB ID: 2ZCO) and SarA (PDB ID: 2FNP) proteins of *S. aureus*

| Compound name	Molecular formula	Molecular weight	Binding affinity (kcal/mol)	
			CrtM	**SarA**
Linalool	$C_{10}H_{18}O$	154	-5.8	-4.5
cis-Verbenol	$C_{10}H_{16}O$	152.3	-6.2	-5.1
Citral	$C_{10}H_{16}O$	152	-6.6	-4.4
γ-Elemene	$C_{15}H_{24}O$	204	-8.1	-5.1
γ-Murrolene	$C_{15}H_{24}O$	204	-7.0	-5.5
Germacrene D	$C_{15}H_{24}O$	204.35	-6.9	-5.7
β-Humulene	$C_{15}H_{24}O$	204.35	-7.6	-5.9
Caryophyllene	$C_{15}H_{24}O$	204.35	-7.6	-6.1
Isocaryophyllene	$C_{15}H_{24}O$	204.35	-7.6	-6.1
Aromandendrene	$C_{15}H_{24}O$	204.35	-7.3	-5.9
Alloaromadendrene oxide	$C_{15}H_{24}O$	204.35	-7.5	-5.4
Ciprofloxacin	$C_{17}H_{18}FN_3O_3$	331.34	-7.6	-5.4
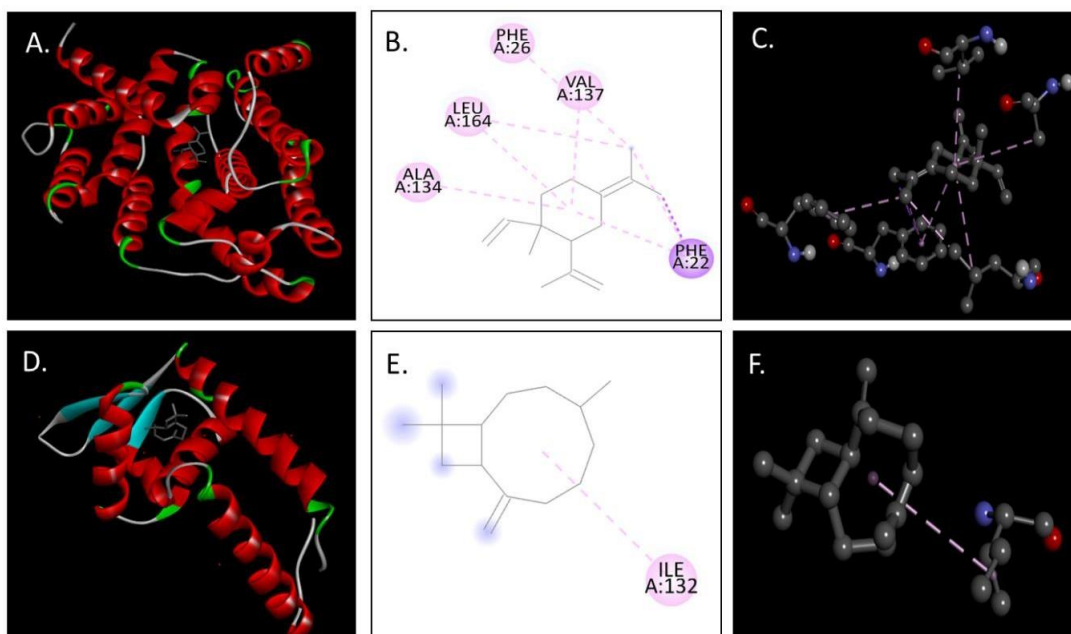
Fig. 4.9 A. B. C- Depiction of binding affinity of CrtM (PDB ID-2ZCO) with γ-elemene and D.E.F- Binding affinity of SarA proteins (PDB ID- 2FNP) with caryophyllene

4.7.3 Molecular dynamics and simulation

Molecular dynamics (MD) and simulation studies were carried out in order to determine the stability and convergence of 2FNP-Caryophyllene complexes. Simulation of 100 ns displayed stable conformation in terms of root mean square deviation (RMSD) values. The RMSD of Cα-backbone of 2FNP bound to Caryophyllene-ligand exhibited a deviation of 2.4 Å after 45 ns, while, the Caryophyllene-ligand showed RMSD 2.5 Å from 12 ns onwards (Fig. 4.10A). From the above, it can be suggested that 2FNP-Caryophyllene is quite stable in complex dueto higher affinity of the ligand towards 2FNP. The plot for root mean square fluctuations (RMSF) indicates the residual fluctuations due to conformational variations into different secondary structures. From the RMSF plot, it was observed that the fluctuation occurs in the residue range from 10-20, 40-58, and 128-140 of target proteins. The highest fluctuating peaks might be due to higher ordered flexibility conforming into loops (Fig. 4.10B). Since, the fluctuating residues in the protein are very less, therefore it implies that the binding of 2FNP and Caryophyllene has significance rigidity. Radius of gyration (Rg) is the measure of compactness of the protein. Here in this study, 2FNP Cα-backbone bound to Caryophyllene ligand displayed lowering of radius of gyration

(Rg) from 16.8 to 16.3 Å (Fig. 4.10C). Significantly lowering radius of gyration (Rg) indicates highly compact orientation of the protein in ligand bound state. Interestingly, we have not noticed any interaction of hydrogen bonds between the ligand and binding site residues of protein. It is clearly visible from the Fig. 4.10D, that in the unbound state of caryophyllene with 2FNP displayed high surface area accessible to solvent in all the cases (Fig. 4.10D). The SASA value is lowered when the receptor is present in the bound state (black line) with the ligand as compared to unbound state (red line) (Fig. 4.10D).

Molecular dynamics (MD) and simulation studies were also carried out in order to determine the stability and convergence of 2ZCO-γ-elemene complex. Simulation of 100 ns displayed stable conformation while comparing the root mean square deviation (RMSD) values. The RMSD of Cα-backbone of 2ZCO bound to γ-elemene complex-ligand exhibited a deviation of 2.1 Å (Fig 4.10E), while, the ligand RMSD of ligand depicted as 3.8.0 Å (Fig. 4.10F). Stable RMSD plot during simulation signify a good convergence and stable conformations. Therefore, it can be suggested that γ-elemene bound to 2ZCO is quite stable in complex due to higher affinity of the ligand. The plot for root mean square fluctuations (RMSF) indicates the residual fluctuations due to conformational variations into different secondary structures. Here, RMSF plot displayed fluctuating residues while high fluctuations observed in the ranges 50-60, 110-130 and 240-260 residual positions (Fig.4.10F). The highest fluctuating peaks comprised of 3.8 Å to 6.7-6.8 Å, might be due to higher ordered flexibility conforming into loops (Fig.4.10B). Therefore, the protein 2ZCO is having significant flexibility to conform into specific secondary structures in order to accommodate the ligand. From the Fig. 4.10G, it was observed that 2ZCO Cα-backbone bound to γ-elemene ligand displayed lowering of radius of gyration (Rg) from 22.1 to 21.8 Å (Fig. 4.10G) indicating highly compact orientation of the protein in ligand bound state. In our study, we have not observed any significant hydrogen bonds between ligand and protein. The overall study of Rg signifies the ligands binding compel the respective proteins to become more compact and less flexible. Followed by Rg analysis, similar pattern was also observed in Solvent accessible surface area (SASA) in both ligand bound and unbound state. It is clearly visible from the Fig. 4.H that in the unbound state of γ-elemene to receptor the protein 2ZCO displayed high surface area accessible to solvent (red line). The SASA value is lowered in bound state whereas it is higher in case of unbound state (black line). Thus, the molecular dynamic simulation study reveals the

potential of 2ZCO bound to γ-elemene and 2FNP bound to caryophyllene possessing high affinity of binding to the protein as well as imparting potent efficiency in binding to the selected protein thereby forming stable protein-ligand complexes [272].
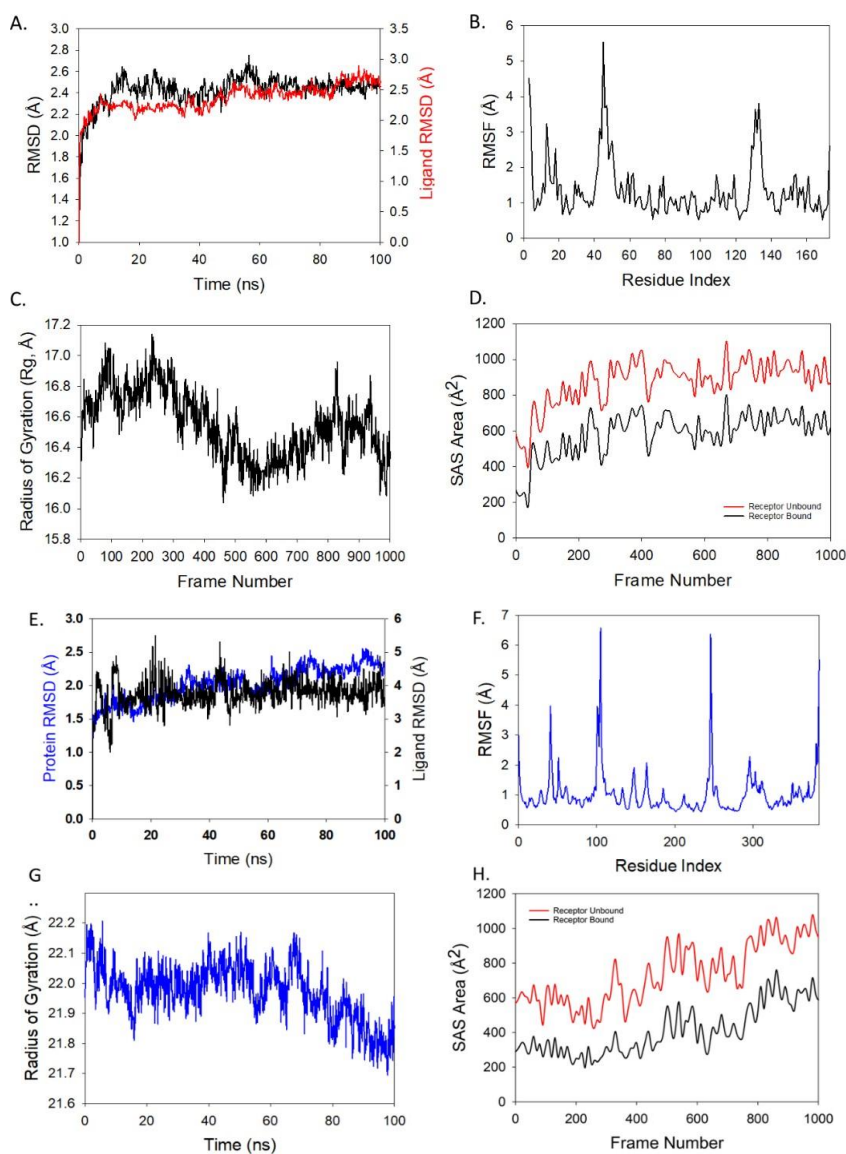

Fig. 4.10 RMSD plots of 2FNP-Caryophyllene where black plot is of protein and red plot is for ligand. (B) RMSF of Cα backbone of 2FNP bound to Caryophyllene-ligand, (C) Radius of gyration (Rg) of Cα backbone of 2FNP bound to Caryophyllene-ligand (D) Solvent accessible surface area of 2FNP bound to Caryophyllene-ligand. MD simulation analysis of 100 ns trajectories of (E) Cα backbone of 2ZCO bound to γ-elemene ligand, (F) RMSF of Cα backbone of 2ZCO bound to γ-elemene -ligand, (G) Radius of gyration (Rg) of Cα backbone of 2ZCO bound to γ-elemene (H) Solvent accessible surface area of 2ZCO bound to γ-elemene.

4.7.3.1 Molecular Mechanics Generalized Born Surface Area (MM-GBSA) calculations

Utilizing the MD simulation trajectory, the binding free energy along with other contributing energy in form of MM-GBSA was determined for both 2FNP-Caryophyllene and 2ZCO-γ-elemene complexes. The results suggested that, for 2FNP-Caryophyllene, the maximum contribution to ΔG_{bind} in the stability of the simulated complexes were due to $\Delta G_{bind}Coulomb$, $\Delta G_{bind}vdW$, $\Delta G_{bind}H_{bond}$ and $\Delta G_{bind}Lipo$, while, $\Delta G_{bind}Covalent$ and $\Delta G_{bind}SolvGB$ contributed to the instability of the corresponding complex. 2FNP-Caryophyllene complex has significantly higher binding free energies dGbind = -74.85±6.79 (Table 5). Having high affinity of binding to the protein as well as efficiency in binding to the selected protein and the ability to form stable protein-ligand complexes. On the other hand, for 2ZCO-γ-elemene, the maximum contribution to ΔG_{bind} in the stability of the simulated complexes were due to $\Delta G_{bind}Coulomb$, $\Delta G_{bind}vdW$, $\Delta G_{bind}H_{bond}$ and $\Delta G_{bind}Lipo$, while, $\Delta G_{bind}Covalent$ and $\Delta G_{bind}SolvGB$ contributed to the instability of the corresponding complex. The binding free energies dGbind for 2ZCO-γ-elemene was found to be -52.23±5.12 kcal/mol. These results supported the potential of Caryophyllene with 2FNP and γ-elemene with 2ZCO to form stable protein-ligand complexes. The overall results of MM-GBSA are given in Table 4.10.

Time series analysis of 2FNP-Caryophyllene and 2ZCO-γ-elemene complexes exhibited the frames captured at different time scale from initial stage to final 100 ns. (Fig. 4.10). Caryophyllene at the binding pocket of 2FNP exhibited the movement from initial 0 ns to 100 ns (Fig. 4.10A). Interestingly, at 50ns caryophyllene moved at the deep core and finally relaxed and better oriented at the 100 ns (Fig. 4.11A). For γ-elemene bound 2ZCO, most of the frames exhibited the stable orientation of the ligand at the binding cavity of 2ZCO (Fig. 4.11B). Except a loop orientation at 100ns at ligand binding state, where at the beginning a small turn observed (Fig. 4.11B) no significant ligand movement is seen.

Principal component analysis (PCA) based Free energy landscape was employed in the present study to elucidate the correlation between statistically significant conformations, representing major global motions observed throughout the trajectory. In the context of molecular dynamics (MD) simulations, PCA was applied to the trajectories of 2FNP-Caryophyllene and 2ZCO-γ-elemene complexes. This analysis

aimed to decipher the randomized global motion patterns exhibited by the atoms of the amino acid residues. The mobility of internal coordinates in three-dimensional space over a temporal span of 100 nanoseconds was first recorded. These data were then organized into a covariance matrix, thus allowing to discern the rational motions within each trajectory in the form of orthogonal sets, which are often referred to as Eigen vectors. In the trajectories of both 2FNP-Caryophyllene and 2ZCO-γ-elemene, the PCA analysis revealed the presence of statistically significant conformations. This analysis enabled to pinpoint the principal motions occurring within the trajectory, including critical motions that are essential for inducing conformational changes. Within the 2FNP-Caryophyllene complex, emergence of four distinct clusters along the PC1 and PC2 plane were observed. This observation signifies a non-periodic conformational transition occurring in the system at 25, 50 and 75 ns and achieving local minima, while later at 100ns large numbers of frames are clustered (Fig. 4.12A). The global minima of protein is achieved at 100ns. While on the other hand, in case of 2ZCO-γ-elemene (Fig. 4.12B), the 2D free energy surface exhibited the clusters of the coordinates of frames achieving due to local minima and randomized motion of the coordinates were observed at 20 and 45ns while at 100ns deep well of global minima is achieved where the conformational variations are least. The convergence of trajectories into a single cluster suggests that the MD trajectories exhibit periodic motion, which is attributed to the presence of stable global conformational changes.

Table 4.10 Calculated Binding free energy components for the 2FNP-Caryophyllene and 2ZCO- γ-elemene.

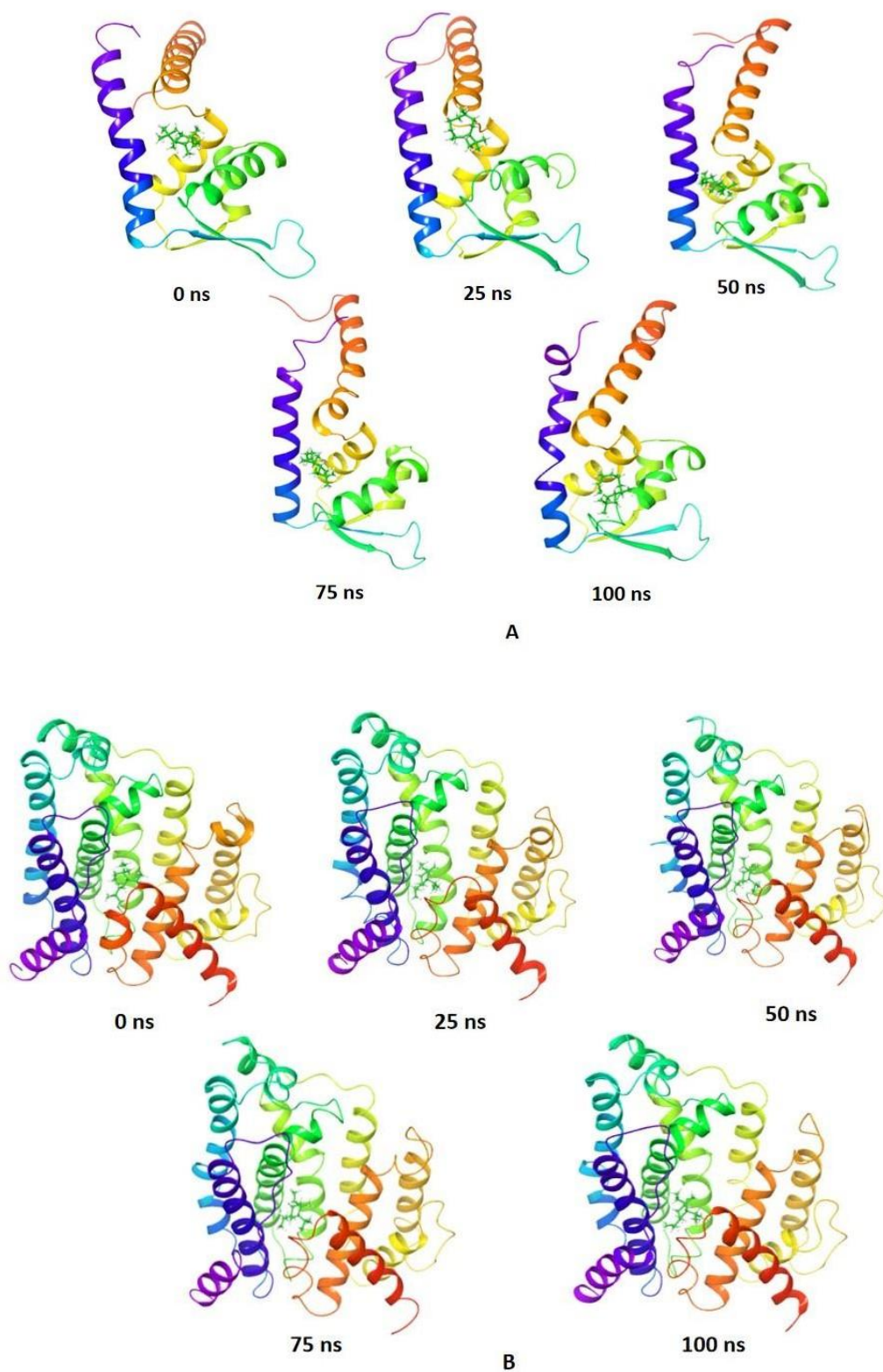| Energies (kcal/mol)	2FNP- Caryophyllene	2ZCO- γ-elemene
ΔG_{bind}	-74.85±6.79	-52.23±5.12
$\Delta G_{bind}Lipo$	-26.18±1.04	-12.23±2.19
$\Delta G_{bind}vdW$	-56.19±2.18	-41.12±1.08
$\Delta G_{bind}Coulomb$	-12.27±6.20	-27.41±2.29
$\Delta G_{bind}H_{bond}$	-1.93±0.34	-3.13±1.32
$\Delta G_{bind}SolvGB$	12.34±3.34	35.41±1.57
$\Delta G_{bind}Covalent$	5.83±4.51	5.91±2.61

Fig. 4.11 Time series analysis of the (A) 2FNP-Caryophyllene and (B) 2ZCO-γ-elemene complexes exhibiting the poses of ligands at various time scale snapshots.
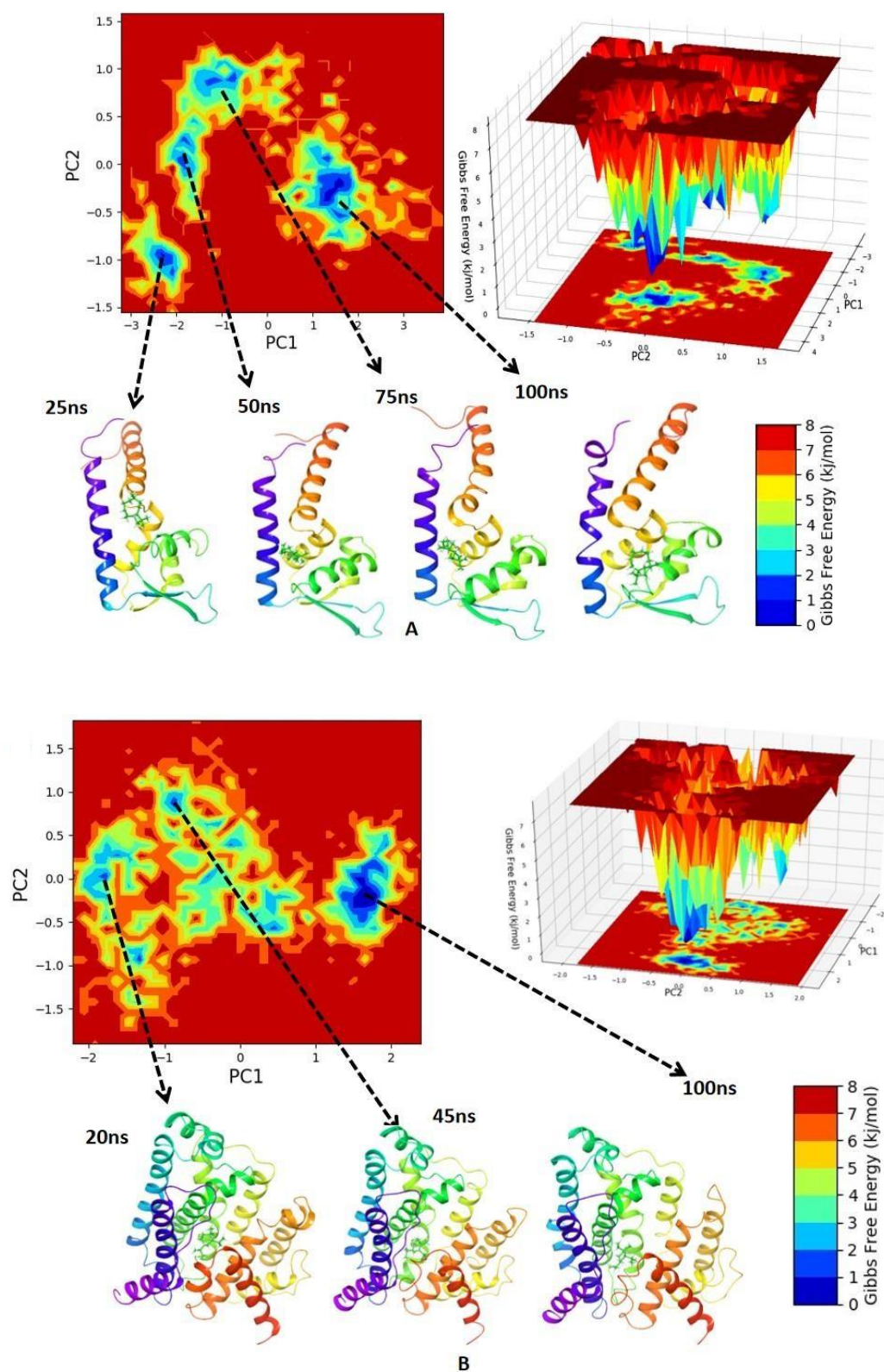
Fig. 4.12 Free energy Landscape (FEL) represented (A) for 2FNP-Caryophyllene and (B) 2ZCO-γ-elemene where left panel exhibiting 2D FEL and the clusters of frames. The structures at mid-point has been exhibited with time scale and the right panel exhibiting the well of global minima in 3D representation.

4.8 Formulation of topical ointment

4.8.1 Physiochemical standardisation of the topical ointment

Table 4.11 demonstrates the physical characterization of the formulated ointment, revealing good appearance, homogenous in nature, and have a stable shelf life. The formulations (2%, 4%, 6%, and 10%) demonstrated good release with pH value of 5.39±0.01, 5.68±0.01, 5.77±0.01and 6.05±0.01 respectively, spreadibility values of 17.2±0.01, 17.2±0.01, 17.4±0.01 and 35.71±0.04 g*cm/sec respectively and viscosity of 26880±0.01, 54200±0.01, 83600±0.01 and 9590±0.01 cp respectively. The formulation showed no presence of any particulate matter and has no phase separation. All these test parameters depicts that the herbal formulation ointment have efficient pharmaceutical characteristics [238].

Fig. 4.13 Different concentration of *K. galanga* L. essential oil topical formulation

Table 4.11 Pharmaceutical evaluation of the formulation

Sl. No	Topical formulation	Physical Appearance	pH	Spreadibility (g*cm/sec)	Grittiness	Viscosity (cp)	Phase Separation
1	2%	Soft and fatty, light yellow and homogenous	5.39±0.01	17.2±0.01	No	26880±0.01	No
2	4%	Soft and fatty, light yellow and homogenous	5.68±0.01	17.2±0.01	No	54200±0.01	No
3	6%	Soft and fatty, light yellow and homogenous	5.77±0.01	17.4±0.01	No	83600±0.01	No
4	10%	Soft and fatty, light yellow and homogenous	6.05±0.01	35.71±0.04	No	9590±0.01	No

4.9 Animal model study of the topical ointment

4.9.1 Skin irritancy

In skin irritancy (Fig. 4.14) no oedema and erythema signs were observed in 72 hours of experimentation. Skin irritation is a local inflammation resulting from direct skin injury, which can be a single, repeated, or prolonged contact with a chemical substance. This study used a rat model for skin irritation and dermal toxicity studies, as rats are known to respond to therapies and their toxic effects similarly to humans. The skin irritation test revealed that the ointment was not an irritant, as no erythema or oedema were observed in the test group and the positive control mupirocin, used in the experiment. The erythema and oedema scores were all zero. This model is used for future predictive studies and for predicting potential toxicity of agents when administered to humans [241].

4.9.2 Dermal toxicity

The study evaluated the acute dermal toxicity of the formulated ointment, following OECD guidelines, and compared it to mupirocin ointment as a positive control. Rats in all groups showed no behavioural changes or irritation signs during the 14-day

experimental period. They were alert, painless to touch, and able to feed themselves well. No abnormal findings from a gross pathological were found in any of the rats' sites. The rats scored zero according to Draize scoring system as it showed zero signs of oedema and erythema as shown in Fig. 4.13. This study highlights the importance of evaluating acute dermal toxicity in wound healing formulations [242].
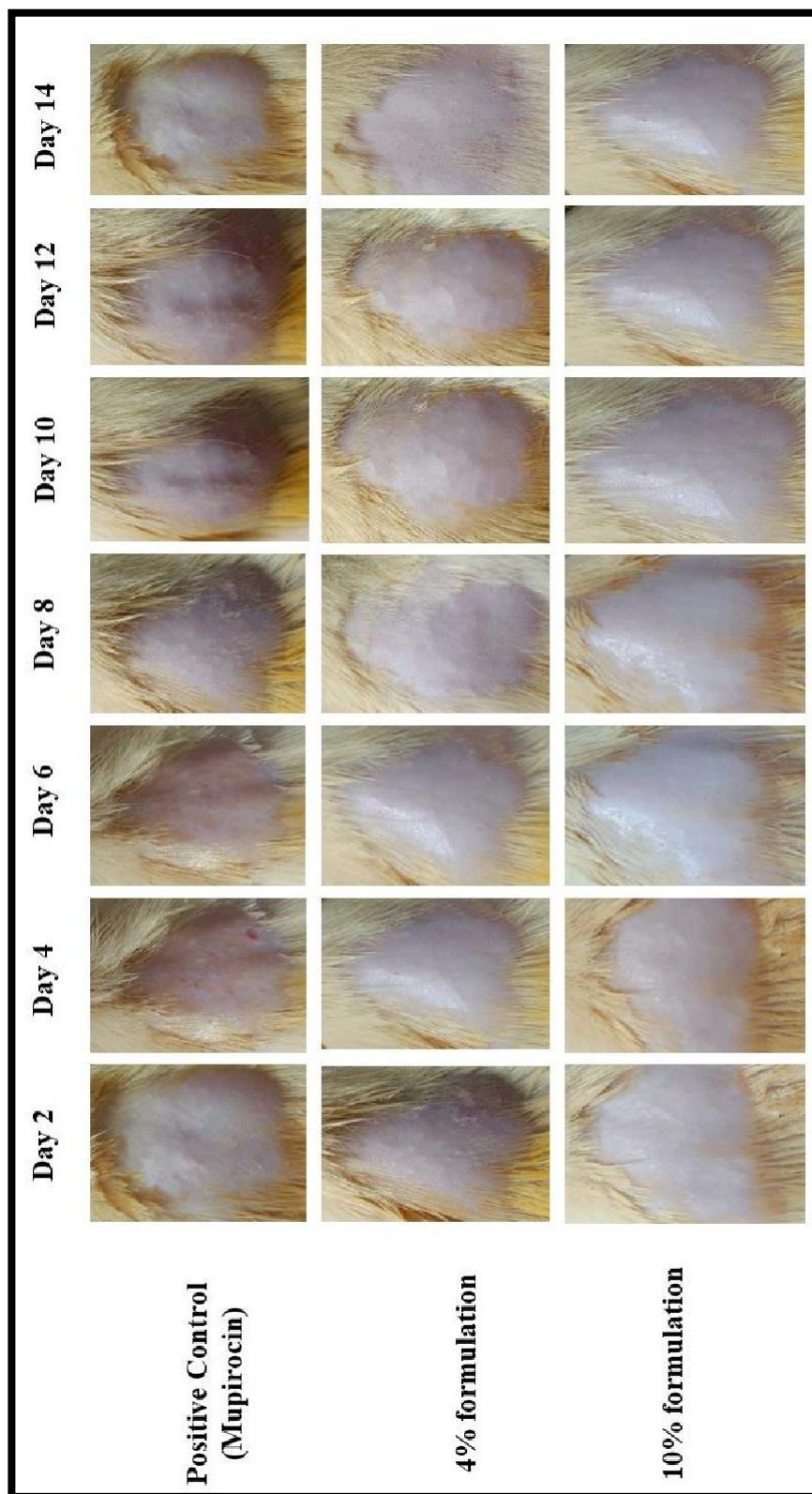
Fig. 4.14 Skin irritancy and acute dermal toxicity showing no signs of oedema and erythema upon treatment with topical application

4.9.3 Wound contraction rate

The prepared herbal formulation of 4% and 10% (w/w) demonstrated 94.47% and 96.51% wound contraction on the 10th day and 100% wound contraction on the 14th day of the treatment in comparison to the standard marketed 2% mupirocin ointment that showed 84.40% wound contraction on the 10th day (Fig. 4.15). The p-value was found to be 0.0001 depicting the results are highly significant. *Staphylococcus aureus* is the most common pathogen involved in wound infection posing a major threat in management of chronic infection as it can lead to bacteremia or sepsis once it enters into the bloodstream. *S. aureus* is known to form biofilms at the site of wound infection delaying the wound healing process. In our study it has been observed that, according to in-vitro studies the essential oil isolated from *K. galanga* L. has efficiently inhibited the biofilm formation and corelated with the in-vivo studies where the topical application of ointment (4% and 10% w/w) formulated from the essential oil has effectively accelerated the wound healing process compared to the standard ointment, mupirocin. Therefore, it can be stated that due to emergence of antibiotic resistance, plant-derived product can be an alternative for the treatment of wound infection as it is likely to be cost effective, environment friendly and non-allergic for human use.
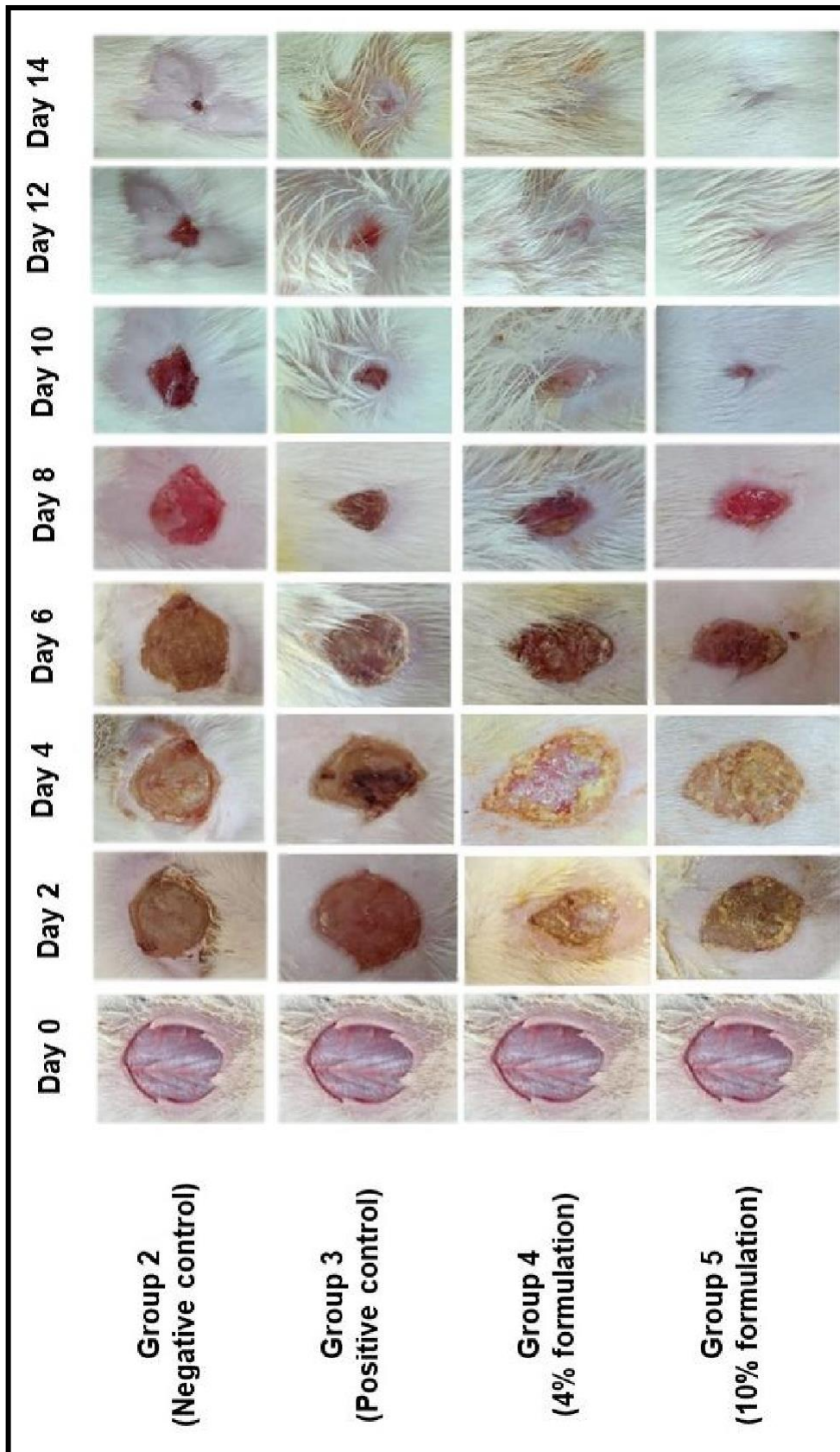
Fig. 4.15 Wound contraction image from day 0 to day 14 post treatment

Table 4.12 Wound contraction rate from day 0 to day 14 after treatment

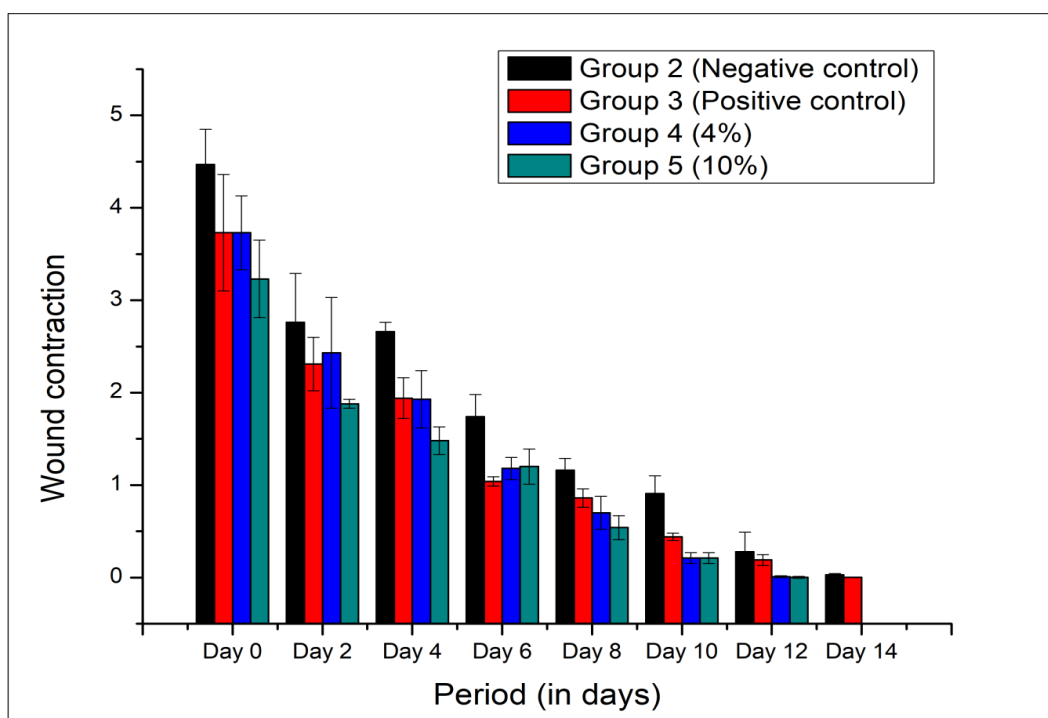| Groups	Group 2 (Negative control)	Group 3 (Positive control)	Group 4 (4% formulation)	Group 5 (10% formulation)
Day 0	4.47±0.38	3.73±0.63	3.73±0.4	3.23±0.42
Day 2	2.76±0.53 (18.75%)	2.31±0.29 (32.47%)	2.43±0.6 (35.69%)	2.43±0.05 (42.64%)
Day 4	2.66±0.1 (36.8%)	1.94±0.22 (44.23%)	1.93±0.31 (48.55%)	1.48±0.15 (53.29%)
Day 6	1.74±0.24 (50.9%)	1.04±0.05 (61.42%)	1.18±0.12 (65.59%)	1.2±0.19 (69.47%)
Day 8	1.16±0.13 (65.2%)	0.86±0.1 (75.5%)	0.7±0.18 (79.53%)	0.54±0.13 (84.1%)
Day 10	0.91±0.19 (78.51%)	0.44±0.04 (89.40%)	0.21±0.06 (94.47%)	0.2±0.04 (96.51%)
Day 12	0.28±0.21 (91.41%)	0.19±0.06 (93.88%)	0.01±0.01 (99.84%)	0.003±0.01 (99.99%)
Day 14	0.03±0.02 (94.52%)	0.0025±0.004 (97.15%)	Line of demarcation, no sign of wound	Line of demarcation, no sign of wound

Fig. 4.16 Analysis graph showing wound contraction of different groups

4.9.4 Histopathology study

Histological sections of the scarred areas of representative rats in each group were stained with hematoxylin–eosin. Hematoxylin–eosin staining of biopsies revealed a complete epithelial regeneration with well-structured layers that cover the entire surface of the wound [273].

Histopathology was conducted on skin samples, supporting the excision experimental study's findings. Photomicrographs stained with H&E demonstrated wound healing phases, with different stages observed among experimental classes. Inflammation, proliferation, and remodelling were documented as wound healingstages among experimental groups.

Due to formation of wound, the layers of skin namely, epidermal layer, dermal layer and hypodermal layer gets ruptured and invasion of pathogen in particular *S. aureus* delay the wound healing process due to the formation of biofilms.

Normal control group depicted the presence of intact epidermal layer, dermal layer and hypodermal layer showing smooth running of fibroblast, sebaceous glands, hair follicle, collagen fibre and network of blood vessels (Fig. 4.17).

It was found that wound healing processes were delayed in the negative control group, while faster remodelling was observed in the test groups. The negative control group experienced delays in wound repair, inflammation, monocyte cells, and cellular necrosis. Histological analysis revealed delayed formation and disorganization of collagen fibers and damage to the epidermis in the untreated group showing distinctive presence of stratified epithelial cells. Hyperplasia of epidermal layer are seen resulting in cell proliferation depicting the group has entered the proliferative stage due to the presence of granulation layer (Fig. 4.18).

In the positive control group, thickness of epidermal layer has subsequently reduced with invasion of newly formed hair follicle in the hypodermal layer. The tissue has now entered into the maturation phase where granulation tissue is replaced by collagen fibres and newly formed glands like sebaceous glands, sweat glands, blood vessels (Fig. 4.19).

In the test group, 4% formulation, it was observed that the skin layers were restored, the layer shows presence of granulation layer depicting the tissue is still in the proliferative phase. It was also possible to observe newly formed hair follicles, sebaceous glands and the arrangement of collagen was comparatively less (Fig. 4.20).

In 10% formulation group, the epidermis and dermis were clearly differentiated, and the skin accessories found were blood vessels, collagen fibres, newly formed hair follicle, fibroblast, glands like sebaceous glands and sweat glands depicting the tissue has entered the maturation phase, thereby produced a skin with significant healing property (Fig. 4.21).
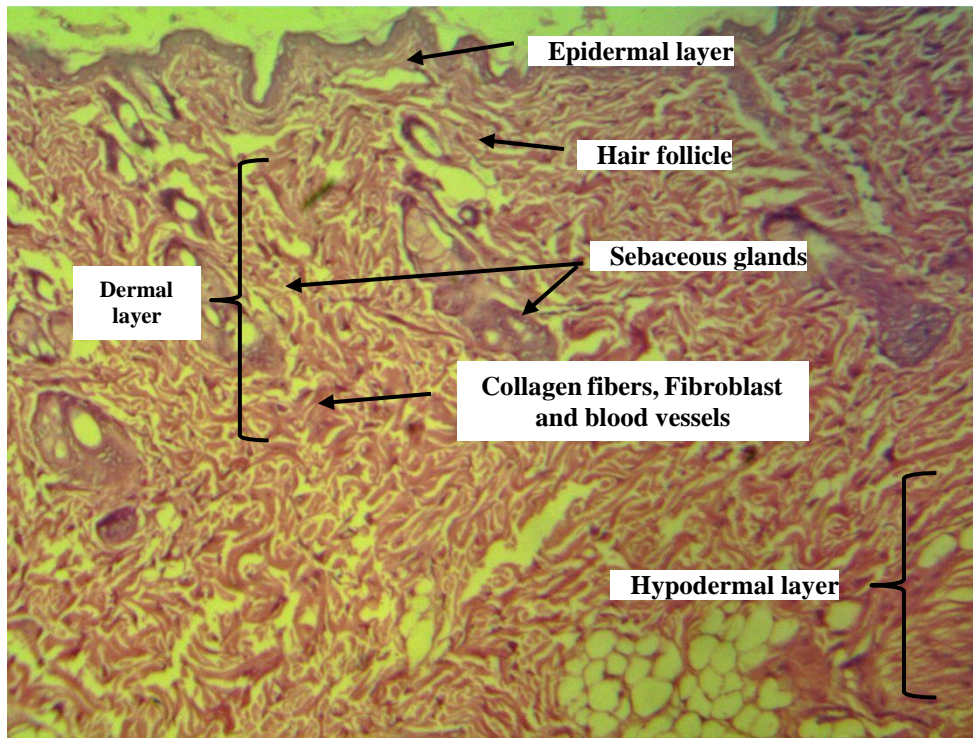
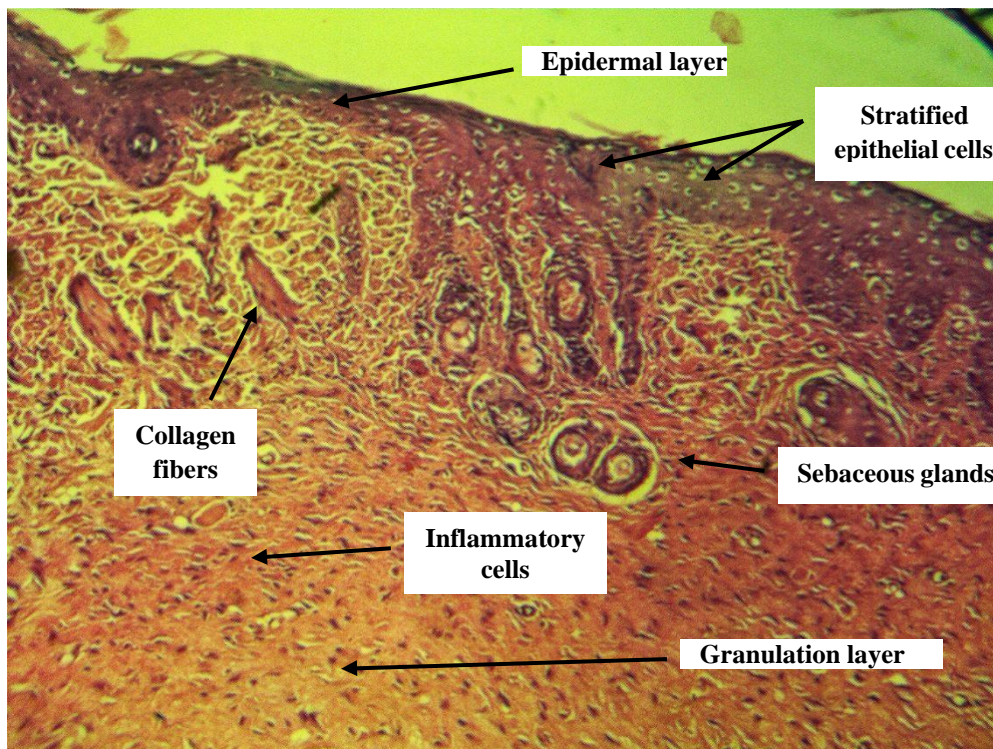**Fig 4.17** Photograph of normal control H&E (X100)

Fig 4.18 Photograph showing wound healing of negative control group
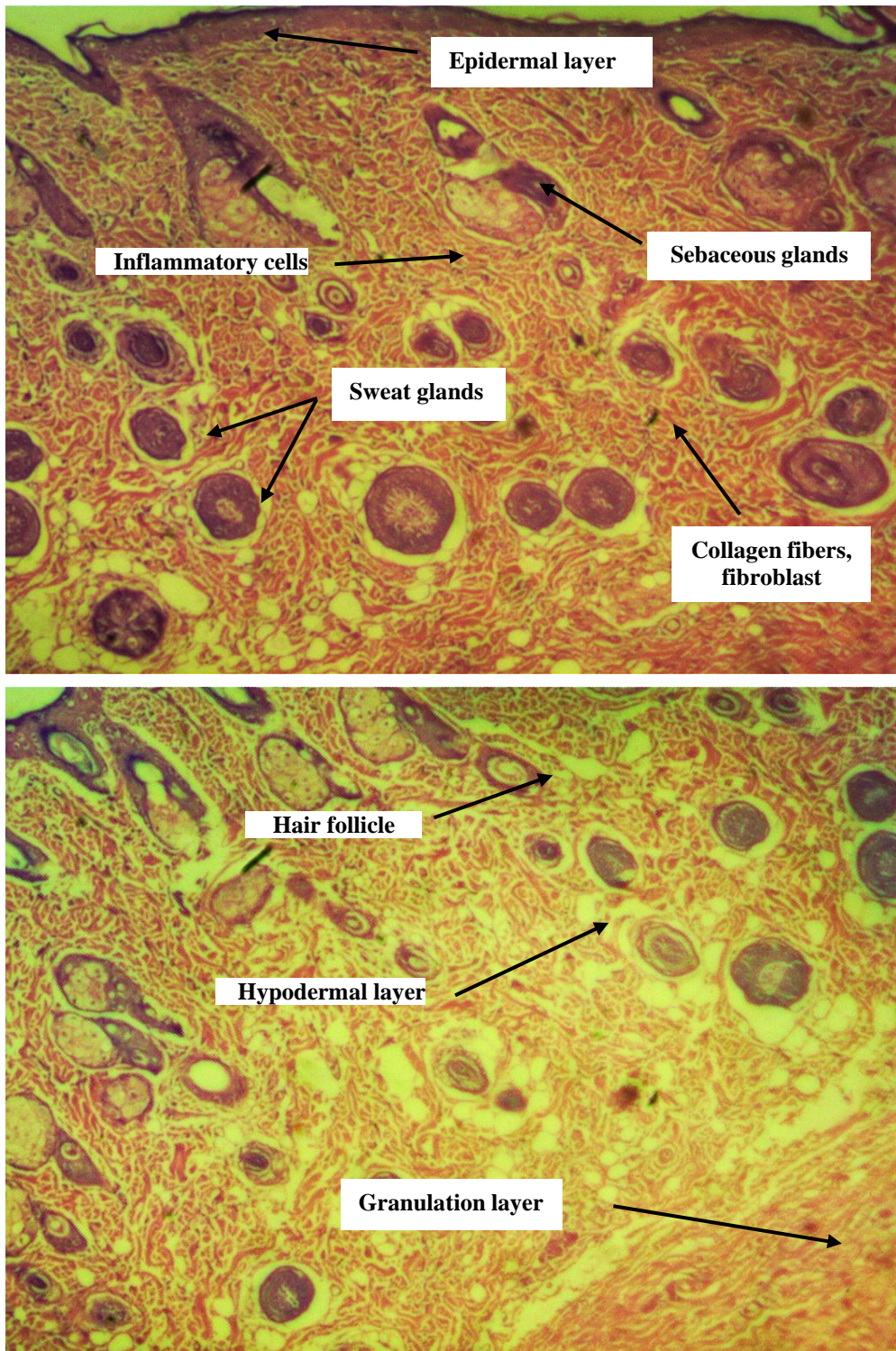H&E (X100)

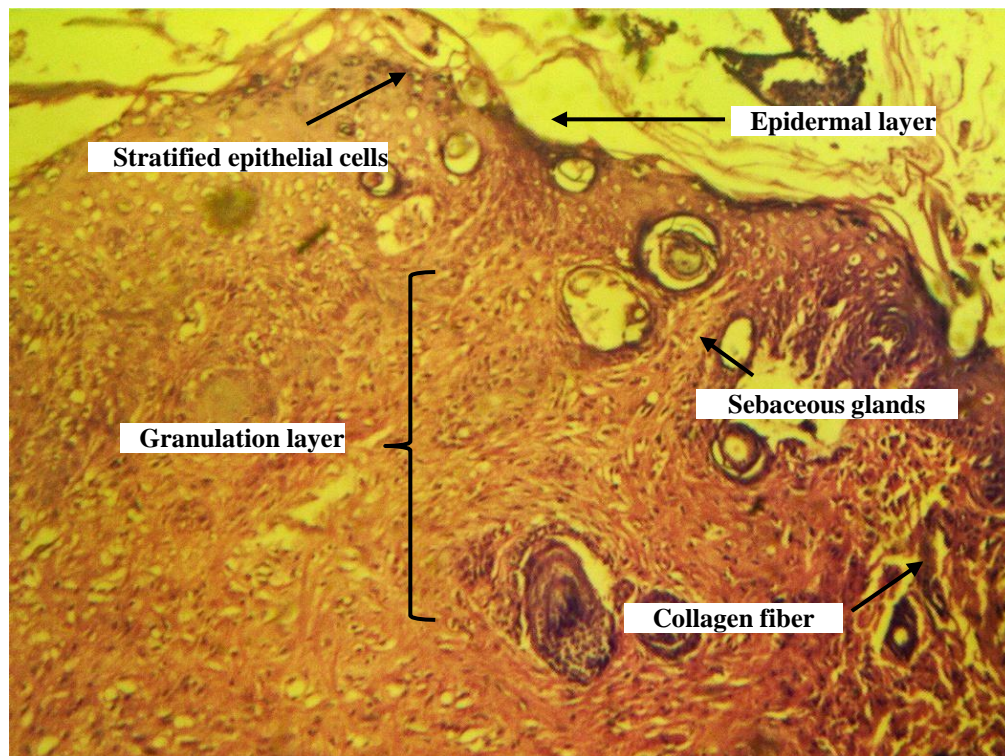**Fig 4.19** Photograph showing wound healing of positive control group treated with 2% Mupirocin H&E (X100)

Fig 4.20 Photograph showing wound healing of group treated with 4% formulation
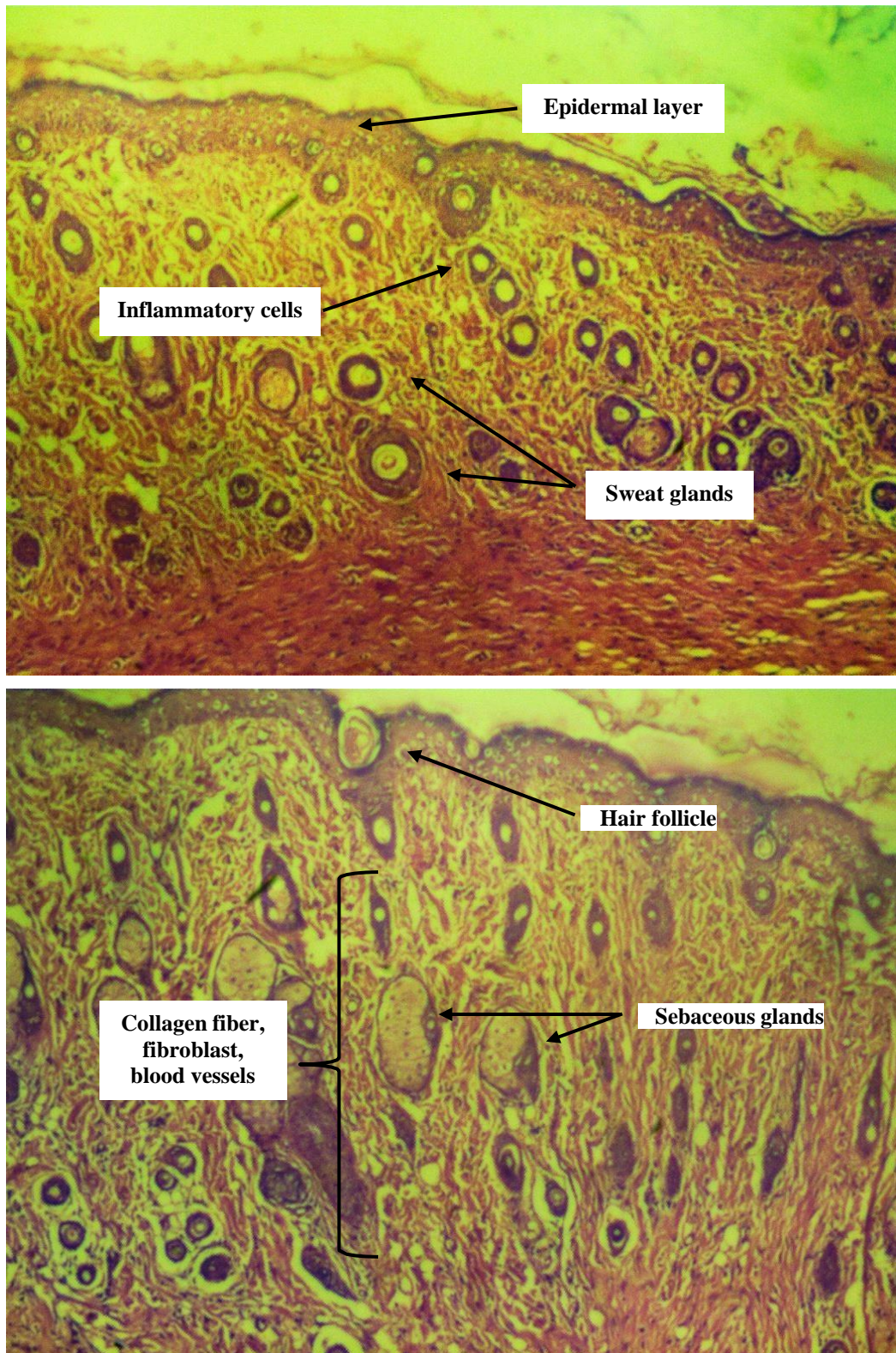H&E (X100)

Fig 4.21 Photograph showing wound healing of group treated with 10% formulation H&E (X100)

This page is intentionally left blank